



Groundwater flow in the transition zone between freshwater and saltwater: a field-based study and analysis of measurement errors

Vincent E. A. Post^{1,2} · Eddie Banks² · Miriam Brunke³

Received: 20 April 2017 / Accepted: 6 January 2018 / Published online: 9 February 2018
© Springer-Verlag GmbH Germany, part of Springer Nature 2018

Abstract

The quantification of groundwater flow near the freshwater–saltwater transition zone at the coast is difficult because of variable-density effects and tidal dynamics. Head measurements were collected along a transect perpendicular to the shoreline at a site south of the city of Adelaide, South Australia, to determine the transient flow pattern. This paper presents a detailed overview of the measurement procedure, data post-processing methods and uncertainty analysis in order to assess how measurement errors affect the accuracy of the inferred flow patterns. A particular difficulty encountered was that some of the piezometers were leaky, which necessitated regular measurements of the electrical conductivity and temperature of the water inside the wells to correct for density effects. Other difficulties included failure of pressure transducers, data logger clock drift and operator error. The data obtained were sufficiently accurate to show that there is net seaward horizontal flow of freshwater in the top part of the aquifer, and a net landward flow of saltwater in the lower part. The vertical flow direction alternated with the tide, but due to the large uncertainty of the head gradients and density terms, no net flow could be established with any degree of confidence. While the measurement problems were amplified under the prevailing conditions at the site, similar errors can lead to large uncertainties everywhere. The methodology outlined acknowledges the inherent uncertainty involved in measuring groundwater flow. It can also assist to establish the accuracy requirements of the experimental setup.

Keywords Groundwater density/viscosity · Equipment/field techniques · Groundwater flow · Salt-water/fresh-water relations · Australia

Introduction

Knowledge of flow patterns in coastal aquifers is a prerequisite to assessing the risk of salinisation to freshwater resources, as well as determining the fluxes of groundwater, and the solutes contained in it, into the ocean. The quintessential conceptual

model for an aquifer connected to the sea is that freshwater flows towards the coast on top of a wedge of intruded seawater. As dissolved salts from the seawater are entrained in the outflowing freshwater, the seawater in the wedge must flow landward to maintain mass balance.

The general validity of this model has been confirmed by numerous studies. Head and salinity measurements from monitoring well transects perpendicular to the shore in a coastal aquifer in the Biscayne area in Florida, USA were analysed in studies by Cooper (1959) and Kohout (1960), which formed perhaps not the earliest (Cooper 1964), but certainly the best-known works in which the model was postulated. Henry (1964) theoretically confirmed the presence of the circulatory flow pattern in the seawater wedge using a semi-analytical solution. This model became known as the Henry Problem and has been replicated repeatedly using numerical codes (e.g. Segol 1994; Simpson and Clement 2004; Abarca et al. 2007). In one of the earliest numerical modelling studies of seawater intrusion, Lee and Cheng (1974) replicated the flow and salinity distribution in the Biscayne aquifer in Florida.

Electronic supplementary material The online version of this article (<https://doi.org/10.1007/s10040-018-1725-2>) contains supplementary material, which is available to authorized users.

✉ Vincent E. A. Post
vincent.post@bgr.de

¹ Federal Institute for Geosciences and Natural Resources (BGR),
Stilleweg 2, 30655 Hannover, Germany

² School of the Environment, Flinders University, GPO Box 2100,
Adelaide SA 5001, Australia

³ Amsterdam, The Netherlands

Numerical models have since then become standard tools to analyse seawater intrusion problems (Werner et al. 2013). Smith (2004) noted though that most numerical studies of the saltwater wedge focused on simulating the thickness, shape and inland extent, and that few had focused on its internal flow dynamics. Chang and Clement (2013) noted a similar paucity of laboratory-sand-tank experiments. A comprehensive survey of the literature for the present article in a search for field studies of flow processes within and near the wedge also yielded fewer studies than expected. An exception is formed by studies of beach water table dynamics and local-scale submarine groundwater discharge that aim to quantify the flux of terrestrial groundwater towards the marine environment (e.g. Baldock et al. 2001; Urish and McKenna 2004; Michael et al. 2005; Gibbes et al. 2007), but interpretations of field data to infer flow patterns at the scale of hundreds of metres or more, appear to be much rarer.

Luszczynski (1961) analysed the head gradients and velocities using data along a groundwater well transect of a freshwater lens across the coastal dunes in the Netherlands. Luszczynski and Swarzenski (1966) presented the head and salinity patterns along a number of cross-sections in Long Island, USA, and inferred flow directions and rates of saltwater intrusion from their data. Acworth (2007) used a bundled piezometer connected to a multi-channel manometer board to infer vertical flow across a freshwater–saltwater interface in northern New South Wales, Australia. Perhaps the paucity of similar studies is explicable by the well-known difficulties of relating heads to flow patterns in systems of variable density groundwater (Luszczynski 1961; Davies 1987; Post et al. 2007)—for example, Hodgkinson et al. (2007) refrained from quantitative analysis of available head data for this reason, and made inferences of the flow patterns below a sandy island in Queensland, Australia, based on hydrochemical patterns instead.

The majority of studies of coastal aquifer systems use numerical models to analyse flow and salinity patterns, and the main purpose of the field data is for calibration and validation. Such models enable the comprehensive analysis of the system, but they are predicated on a preconceived conceptual model, and require making simplifying assumptions—for example, the transient effects due to tides or recharge variations are often ignored in numerical models (Werner et al. 2013). Direct analysis of field data therefore remains necessary to validate and improve the conceptual thinking about groundwater flow in aquifers near the coast.

This study presents data from a coastal aquifer in South Australia where a dedicated groundwater monitoring network was installed to study the seawater intrusion interface. The original motivation of the study was to quantify the flow dynamics, as the site provides an interesting addition to existing case studies, because the salinities in the bottom of the aquifer are much higher than seawater. Such complex stratified

mixing zones have thus far only been studied theoretically in numerical and laboratory studies (Oz et al. 2011, 2014). These latter studies focused on the salinity and flow dynamics in an aquifer connected to a meromictic (i.e. stratified) lake, and showed that the thickness and density of the surface-water layers exert an important control on the groundwater processes in the aquifer. The source of the hypersaline groundwater in the present study area remains unknown to date, and establishing the flow direction could confirm if it originates from a deeper aquifer and ascends by upward flow.

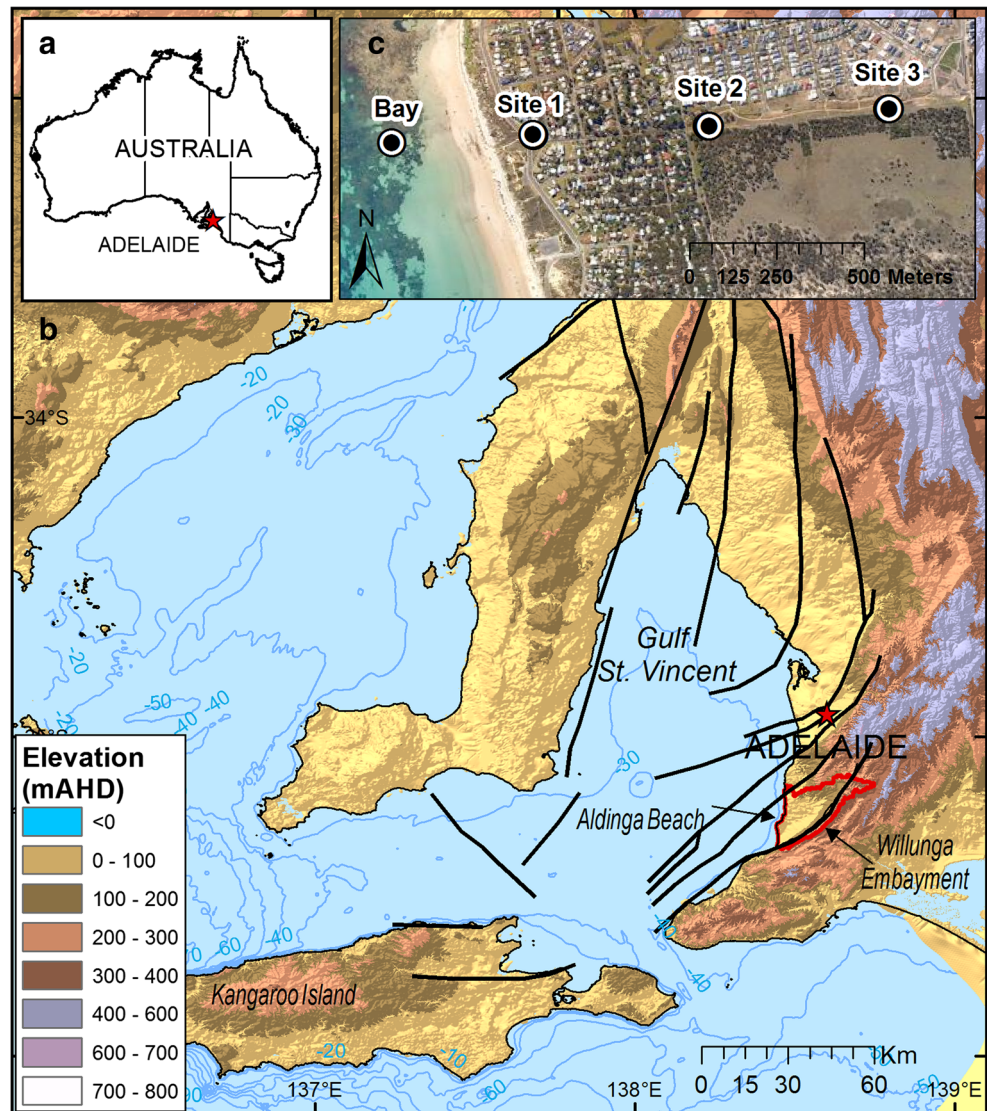
The practical difficulties associated with measuring heads across a freshwater–saltwater interface, such as the effect of a salinity stratification within an observation well (Kohout 1961) have received far less consideration in the literature than the theoretical framework for inferring flow components based on the gradient of the freshwater head (Luszczynski 1961; Davies 1987; Post et al. 2007). The objective of this study is therefore to analyse the various sources of measurement error and the associated uncertainty of the head gradients that indicate the flow direction. A few published works addressed this issue for freshwater flow systems (Silliman and Mantz 2000; Devlin and McElwee 2007), but the quantification of errors related to the necessary density corrections seems to have remained largely neglected thus far.

Study area

The studied groundwater transect is located in the town of Aldinga Beach, which is approximately 50 km south of Adelaide, South Australia (Fig. 1). Groundwater occurs in a series of sedimentary strata that are part of the Willunga Embayment, which is a sub-basin of the larger St Vincent Basin. The sediments in the basin range in age from the late Eocene to Quaternary. From oldest to youngest age, the five most significant geological units are the pre-Cambrian basement rocks, the Maslin Sands Formation, the Blanche Point Formation, the Port Willunga Formation and Quaternary sediments. The Maslin Sands and the Port Willunga Formation are important production aquifers and support widespread irrigation further inland (Adelaide and Mount Lofty Ranges NRM Board 2007). Groundwater abstraction from the fractured basement rocks occurs locally at a smaller scale.

The target of the present study was the Port Willunga Formation (PWF), which mainly consists of calcareous sandstone, sandy limestone and bryozoal limestone, deposited between the late Eocene and middle Miocene (Cooper 1979). The shallowest member of the PWF is ca. 50 m in depth close to the coast but decreases in thickness further inland to ca. 20 m (Fig. 2). The thickness of the second, deeper member varies from 30 to 50 m. The aquifer is covered by Quaternary sediments, which vary in thickness between 15 and 20 m and consist of fine sands, silt and clay. The deepest unit

Fig. 1 **a** The study area location in Australia. **b** Map showing the regional topography and offshore bathymetry (meters relative to Australian Height Datum, m AHD). The red line marks the outline of the Willunga Embayment, black lines are the major regional faults. Inset map **c** shows the location of the observation wells in the town of Aldinga Beach which are presented as a cross section in the subsequent figure. The offshore location labelled “Bay” in **c** marks the point where a pressure transducer was deployed on the seafloor



encountered during drilling was the Chinaman Gully Formation, which is comprised of carbonaceous sands, lignites, silt and clay. This formation forms a thin bed between the PWF aquifer and the underlying Blanche Point Formation, which is recognised as an aquitard between the PWF and the Maslin Sands aquifer below.

The water table is found just near the boundary between the PWF and the Quaternary units, at an elevation near sea level. The Quaternary strata have a low permeability, and perched conditions and surface ponding are common in this area. The horizontal hydraulic conductivity of the PWF has been determined in pumping tests at a nearby managed aquifer recharge site and was found to range between 0.7 and 7 m/day (Irvine 2016). There are no data about the anisotropy of the aquifer.

Hydraulic heads in the PWF vary with the tides in the Gulf St Vincent. The tidal regime is a mixed one (Bowers and Lennon 1990), and is dominated by the diurnal O_1 and K_1 , and the semi-diurnal M_2 and S_2 components. The latter two

have almost the same amplitude, and this results in an exaggerated spring-neap cycle (Bye and Narayan 2009). The amplitude of spring tides at this location is typically 0.5–1 m greater than the average tidal range of about 0.5 m, whereas almost no tidal variation occurs during the so-called dodge tides. Meteorological tides associated with the weather systems moving along the south Australian coast are also significant. While the flow patterns in the aquifer are clearly a function of the tides, the detailed analysis of the propagation of the tidal fluctuations will be dealt with in a separate paper.

The climate is Mediterranean with dry hot summers and mild, wet winters. A weather station is located at the nearby town of Noarlunga that has been operated by the Australian Bureau of Meteorology Mean since the year 2000. The mean annual rainfall is 449 mm year⁻¹, and the yearly averaged daily maximum and minimum temperatures amount to 21.7 and 12.7 °C, respectively (Australian Bureau of Meteorology 2015). The land use along the studied transect is dominated by

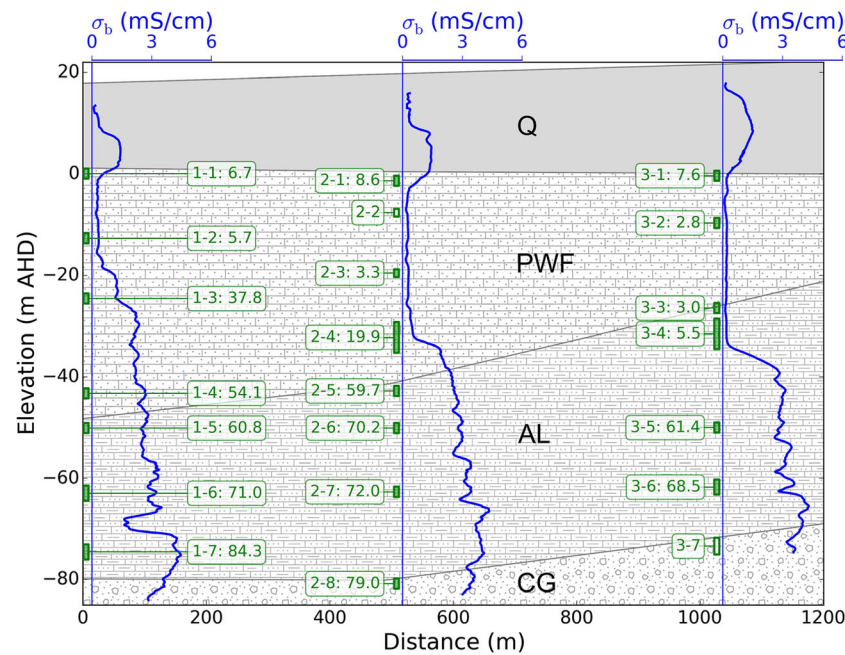


Fig. 2 Cross-section of the observation well transect showing the lithology, screen positions and identifiers. The screens indicated in green were sampled during this study, and the number behind the screen identifier is the specific conductance of groundwater for a reference temperature of 20 °C in mS/cm. The overlying graphs with the blue lines show a bulk conductivity log of the subsurface (σ_b in mS/cm)

recent urban development and bushland with coastal native vegetation.

Methodology

Drilling

A total of 22 observation wells distributed over three sites were installed in multiple nested wells. Drilling of the wells took place in November and December 2012. The sites are numbered consecutively from the coast as sites 1, 2 and 3, and are separated from each other by approximately 500 m (Fig. 2). Site 1 is located 150 m from the mid-tidal line at an elevation of 17.6 m above the Australian Height Datum (AHD, approximately mean sea level). The elevation at sites 2 and 3 is 19.2 m, and 21.1 m above AHD, respectively. A total of seven observation wells have been installed at sites 1 and 3, whereas site 2 has eight observation wells. The well screens are labelled according to their position and depth using a two digit code—for example the code 2–1 refers to the piezometer at site 2 at the shallowest depth, and 2–2 is the label for the next piezometer down. All screens are in the PWF, except the topmost well screen at site 2, which sits in the Quaternary sediments, and the deepest at site 3, which sits in the Chinaman Gully Formation. After drilling, a bulk conductivity, σ_b , log of the subsurface (Reynolds 2005) was determined

using a downhole electromagnetic induction tool at the time of drilling with measurements recorded every 0.1 m depth. Letters in black font indicate the names of the lithological units: Q Quaternary, PWF Port Willunga Formation, AL Aldinga Member of the PWF, CG Chinaman Gully Formation. The specific conductance of seawater in Aldinga Bay is 51 mS/cm

using a downhole electromagnetic induction tool in the deepest open borehole at each site with a vertical resolution of 0.1 m (Fig. 2).

The diameter of the observation wells was 50 mm, and the screen length varied. At each site, three boreholes were drilled, with up to three piezometers per borehole. The screened intervals of these nested piezometers were separated by a cement/bentonite slurry to prevent vertical interaction. The screens of wells 2–2 (site 2) and 3–7 (site 3) were blocked and could therefore not be included in the study. The details of each observation well, including the screen lengths, are included in Table 1. The top of the casing of each observation well was determined using a Trimble real-time kinematic (RTK) geographical positioning system (GPS). The known permanent survey mark that was used as a reference datum for the survey had a precision of ± 25 mm. Due to the open area of the study site, the accuracy of the RTK-GPS measurements was ± 8 mm horizontally and ± 12 mm vertically. The depth of each well was accurately measured using a calibrated steel-weighted drillhole measuring tape to the nearest cm.

Water level measurements

Water level measurements were conducted during the period 12 May to 5 August 2015. Each observation well was equipped with a pressure transducer to determine the water level within the well over time. For most wells, an In-Situ

Table 1 Summary of observation well data. Δx is the distance from site 1. Density of seawater (labelled *Bay*) was measured on a sample taken on 3 June 2015. The logger in observation well 3–6 failed and could not be considered in the analysis. *SD* is the standard deviation

Well	Distance from site 1, Δx (m)	Depth of bottom of well screen, z_i (m AHD)	Well screen length (m)	Average water density, ρ_a (kg/m^3)	Density of water sample, ρ_s (kg/m^3)	Logger pressure offset, P_{offset} (kPa)	Logger clock offset (s)	SD of hydraulic head, σ_h (cm)	SD of freshwater hydraulic head, σ_{hf} (cm)
1–1	0	0.0	2		1,001.5	−3.596	−57	2.0	2.0
1–2	0	−12.7	2	1,000.6	1,001.1	0.222	30	3.0	2.4
1–3	0	−24.6	2	1,014.2	1,018.8	−0.096	−82	1.1	3.2
1–4	0	−43.3	2	1,000.8	1,028.5	−0.025	−96	2.0	4.8
1–5	0	−50.1	2	1,023.9	1,032.3	0.032	−84	4.0	5.4
1–6	0	−63.0	3	1,021.5	1,037.8	0.080	−50	1.4	6.6
1–7	0	−74.5	3	1,033.3	1,046.3	0.471	−89	1.3	7.7
2–1	503	−1.3	2	–	1,002.7	−0.039	−84	5.0	2.0
2–3	503	−19.6	1.5	1,000.1	1,000.5	0.062	−119	1.3	2.8
2–4	503	−32.3	6	1,004.0	1,008.6	0.055	−110	0.2	3.8
2–5	503	−42.8	2	1,023.5	1,031.3	−0.026	−82	2.9	4.7
2–6	503	−50.1	2	1,021.0	1,037.3	−0.066	40	1.6	5.4
2–7	503	−62.7	2	1,024.4	1,038.3	0.000	25	1.6	6.6
2–8	503	−80.8	2	1,041.7	1,042.7	1.943	−144	0.6	8.3
3–1	1,022	−0.3	2	–	1,000.7	0.284	0	3.3	2.0
3–2	1,022	−9.6	2	999.5	999.7	−0.276	0	1.4	2.2
3–3	1,022	−26.5	2	999.7	999.8	0.135	−100	2.7	3.3
3–4	1,022	−31.5	6	999.8	1,001.0	0.898	0	1.9	3.7
3–5	1,022	−50.0	2	1,020.6	1,031.7	0.307	−90	3.7	5.4
3–6	1,022	−61.7	3	1,033.6	1,036.2	–	–	–	–
Bay	−500	–	–	–	1,026.6	–	–	–	–

Level TROLL 300 instrument was used, which record the absolute pressure with a manufactured specified accuracy of 0.2% of the full-scale range of 2.07×10^5 Pa (In-Situ Inc. 2013), i.e. 0.41 kPa which equates to a water column height of 0.04 m. In four wells (3–1, 3–2, 3–4 and 3–6 at site 3) a Van Essen Instruments TD DI241 Diver was used, which has a manufacturer specified accuracy better than 0.005 m (Van Essen Instruments 2004). Both manufacturers report an accuracy of the instruments' temperature sensors of 0.1 °C. The loggers were suspended on high-grade stainless steel wires attached to the well caps, and were sitting at approximately 2 m below the air–water interface. An In-Situ Level TROLL 300 instrument was deployed on the bottom of the Gulf St Vincent at a distance of 350 m from the shoreline to record the surface-water level between 22 May and 18 August 2015 (Fig. 1).

Air pressures were recorded by In-Situ BaroTROLL 500 pressure transducers, with a reported accuracy of 0.1% of the full-scale range of 2.07×10^5 Pa (In-Situ Inc. 2013), i.e. 0.02 m of water. To minimise interference by temperature fluctuations, the instruments were suspended inside observation wells at sites 1 and 3 at a depth of approximately 2 m below the top of the well casing. No significant deviations

between the air pressure loggers were observed during the measurement period and therefore only the measurements at site 1 were used.

The same computer was used consistently to download the field data, and all times were recorded for Australian Central Daylight Time, with daylight savings not in effect. The measurement interval was 2 min, and logs were started at the nearest whole hour when loggers had to be restarted in the field. The potential logger offset and drift were determined by recording the pressure difference (P_{offset}) between each logger and the BaroTROLL at site 1 during the time intervals when loggers were removed from the observation well and were measuring the atmospheric pressure. When the data were downloaded from the loggers, the time difference between the clock of the datalogger and that of the field computer was noted for the Level TROLL instruments. The software for the Diver instruments did not have this functionality.

Electronic dip meters did not work correctly in most of the wells due to the high salinity. Manual measurements of the water levels were conducted instead using a calibrated graduated measurement tape with a brass cylinder (“plover”), which produces an audible noise when it hits the water surface in the well. The manual readings were converted to hydraulic

heads (h) in metres relative to AHD by subtracting the measured distance between the top of the well casing from the elevation of the casing measured with the RTK-GPS. For the purpose of downloading and determining the density measurements described in the following section, the water level loggers had to be removed from the water column.

Density measurements

To determine the density stratification of the water column inside the observation wells, downhole measurements of temperature and electrical conductivity were conducted using a YSI 600 XLM multi-parameter sonde. The sonde was connected to a 150-m-long cable on a motorised winch system and real-time data was viewed on a handheld control unit (YSI 650 MDS). The sonde was lowered down the well to just below the water surface and allowed to equilibrate for 10 min before profiling the water column for pressure, electrical conductivity and temperature at 2-s sample intervals. The manufacturer-specified accuracy is 0.3 m of water for pressure, 1% of the measured value for electrical conductivity and 0.15 °C for temperature (YSI Incorporated 2009). These specifications were not attained, however, as water leaked into the probe when the instrument was deployed in the deeper wells. This led to spurious oscillations of recorded electrical conductivity values and consequently the data of the first two sonde deployments became associated with a large uncertainty.

The depth reported by the sonde is calculated incorrectly because it is based on the measured pressure and the point density (calculated internally based on conductivity and temperature), not the integrated density over the entire water column. Post-processing of the data was therefore necessary to calculate the measurement depths according to:

$$z_d = \int \frac{1}{\rho(P)g} dP \quad (1)$$

where z_d is the depth of a measurement (m), $\rho(P)$ is the measured variation of the density (kg/m^3) as a function of the pressure P (Pa) and g is the gravitational constant (9.81 m/s^2). The integration was done numerically using the SciPy library for the programming language Python (Oliphant 2007; Walt et al. 2011), between the first measurement point, where the probe sat just below the water surface, and each subsequent measurement point until the deepest measurement point was reached.

The average density of the water column inside the observation well was obtained from:

$$\rho_a = \frac{\int \rho(z_d) dz_d}{D} \quad (2)$$

where ρ_a is the average density of the water column (kg/m^3),

$\rho(z_d)$ is the density as a function of depth below the air water interface (kg/m^3), and D is the depth of the deepest measurement below the air–water interface (m). The integration is conducted between the first and last measurement point. Alternatively, ρ_a can be obtained from:

$$\rho_a = \frac{P_D}{Dg} \quad (3)$$

where P_D is the pressure (relative to the atmospheric pressure) at the deepest measurement point below the air–water interface (m).

All the wells were pumped in May 2015 using a Grundfos MP-1 pump and water samples were taken after the well volume was purged at least 3 times and the values of the field parameters, electrical conductivity, temperature, pH and dissolved oxygen as measured in a flow-through cell, became stable. The density of the samples, ρ_s , was measured in the laboratory of the School of the Environment of Flinders University using an electronic density meter (Densito 30PX, Mettler Toledo, Columbus, Ohio). These samples represent the density of the groundwater in the PWF at the depth of the well screens at the time the sample was taken.

Conversion to freshwater head

The conversion of measured pressures to freshwater heads involved several steps aimed at removing any possible systematic errors. Using the manufacturers' provided software, the recorded data were exported to comma separated values files, which were read for further processing using the Pandas library for Python (McKinney 2010). The following post-processing steps were applied to the pressure data:

1. The time offsets that were recorded when downloading the logger data were used to ensure that the timestamps of all logs were synchronised by shifting the time series. The data were then resampled at 2-min intervals starting at a whole hour by linearly interpolating between the measurement values.
2. The measured pressure offset P_{offset} for each logger was added to all measurement values.
3. For some time-series logs, it was necessary to manually shift the data based on a visual inspection of the graphed time series of measured pressures. This was because the loggers were not always redeployed at exactly the same depth as the wire was suspended from the cap of the observation well, which was not always inserted in the same manner by the different operators.
4. Data were deleted during the recorded time periods when the logger was outside the water column of the observation well. To maintain a continuous time series, the deleted data were replaced with interpolated data which were

determined by fitting a spline function through the half-hourly values of a 360-min time period that started 180 min before the logger was lifted from the well (Fig. 3).

5. The barometric pressure time series measured at site 1 was subtracted from the measured total pressure to obtain the pressure due to the weight of the water column above the sensor.
6. Pressures were converted from their reported values in Pascal units to metres of water using the following formula:

$$h_1 = \frac{P_1}{\rho_1 g} \tag{4}$$

where h_1 is the height of the water column above the pressure sensor (m), which has an average density ρ_1 , and P_1 is the pressure relative to the atmospheric pressure (Pa). The values of ρ_1 were determined for the water column within each observation well by evaluating the integral in Eq. (2) between the water surface and the known deployment depth of the logger.

7. To convert the water levels to hydraulic heads relative to m AHD (h), an offset was determined by fitting the time series of h_1 through the manual head measurements using a least squares fitting function. Manual readings for which no electronic pressure transducer value was available within 10 min from the time they were recorded, were not considered in the least-squares analysis. An estimate of the composite measurement error was obtained from the residuals of the least squares fitting function.

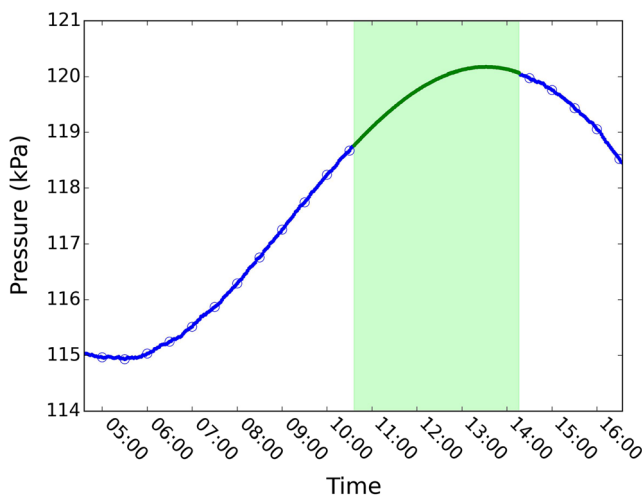


Fig. 3 Graph showing the measured pressures in observation well 1–5 on 12 June 2015 when the logger was removed from the well for a relatively long time period between 10:36 and 14:16. The blue data points are the measured values. The green data points are the interpolated values which were obtained by fitting a fifth-order spline function through the half hourly data points marked by open blue circles. Individual data points are not discernible at this scale as they were recorded every 2 min

8. The freshwater head was calculated using:

$$h_f = \frac{\rho_a}{\rho_f} h - \frac{\rho_a - \rho_f}{\rho_f} z \tag{5}$$

where h (m) is the hydraulic head obtained in step 7, ρ_f is the freshwater density (kg/m^3), and z is the elevation of the bottom of the observation well (m AHD).

Flow components

The strong variation of the groundwater density within the aquifer complicates the interpretation of the flow patterns (Luszczynski 1961). The horizontal and vertical components of the specific discharge were therefore analysed separately following Post et al. (2007). The flux in the horizontal direction at a fixed elevation is given by:

$$q_x = -K_x \frac{dh_f}{dx} \tag{6}$$

where q_x is the horizontal component of the specific discharge vector (m/day), K_x is the horizontal component of hydraulic conductivity in freshwater (m/day), and dh_f/dx is the horizontal gradient of the freshwater head (dimensionless). The x direction was defined as positive in the landward direction, which means that positive values of q_x indicate landward flow.

The vertical flux is given by:

$$q_z = -K_z \left[\frac{dh_f}{dz} + \left(\frac{\rho - \rho_f}{\rho_f} \right) \right] \tag{7}$$

where q_z is the vertical component of the specific discharge (m/day), K_z is the vertical component of hydraulic conductivity in freshwater (m/day), dh_f/dz is the vertical gradient of the freshwater head (dimensionless), and ρ is the groundwater density (kg/m^3).

In practical applications, the gradient dh_f/dz is approximated by its difference form $\Delta h_f/\Delta z$ using the values of h_f and z for two nearby screen pairs. Similarly, the average value of the groundwater density between the two well screens, ρ' , is used for ρ (Post et al. 2007). Since the groundwater density is only known at the elevation of the well screens (from the measurement of ρ_s), there can be considerable uncertainty about the value of ρ' . Therefore, to calculate ρ' , the relationship between the bulk specific conductance, σ_b , measured by downhole geophysical logging at the time the boreholes were drilled (Fig. 2), and the measured density of the water samples ρ_s was determined using linear regression, yielding

$$\rho_s = 998.4 + 0.122\sigma_{b,s} \tag{8}$$

with $R^2 = 0.98$. In this equation, $\sigma_{b,s}$ is expressed in mS/m and the added subscript s indicates that the value represents the

average σ_b over the depth interval of each well screen. The values of σ_b were then converted to density values, which were used to calculate ρ' between pairs of well screens by integration.

With z positive in the upward vertical direction, the vertical component of flow is directed upward if $q_z > 0$, meaning that upward flow will occur when (cf. Eq. 7):

$$-\frac{\Delta h_f}{\Delta z} > \frac{\rho' - \rho_f}{\rho_f} \tag{9}$$

Hydrostatic (no vertical flow) conditions exist when:

$$-\frac{\Delta h_f}{\Delta z} = \frac{\rho' - \rho_f}{\rho_f} \tag{10}$$

Uncertainty analysis

For flow in an aquifer without density variations, the uncertainty of the calculated flux q (in the x or z direction) can be determined using basic error propagation rules (Silliman and Mantz 2000). The flux in the absence of density effects is given by the difference form of Darcy’s law:

$$q_j = -K_j \frac{\Delta h}{\Delta j} = -K_j \frac{h_1 - h_2}{j_1 - j_2} \tag{11}$$

where j represents either the x or z coordinate. The subscripts 1 and 2 denote two adjacent screens, respectively. If the errors in the measurements of h and x or z are random and uncorrelated, the standard deviation of either of the Δ terms (Δh or Δj) in Eq. (10) is

$$\sigma_{\Delta} = \sqrt{\sigma_1^2 + \sigma_2^2} \tag{12}$$

where σ on the right-hand side is the standard deviation of the measurand (h , x or z). The relative error of the gradient $\Delta h/\Delta j$ is:

$$\frac{\sigma_i}{|i_j|} = \sqrt{\left(\frac{\sigma_{\Delta h}}{\Delta h}\right)^2 + \left(\frac{\sigma_{\Delta j}}{\Delta j}\right)^2} \tag{13}$$

where the notation $i_j = \Delta h/\Delta j$ is introduced for brevity.

These simple error propagation rules cannot be used for the vertical flow component in variable-density systems because in the vertical freshwater-head-gradient term, $\Delta h_f/\Delta z$, both h_f and z are affected by the measurement error of z , and hence the measurement errors of these terms are correlated. Therefore, the uncertainty analysis of the q_z term was conducted using a Monte Carlo analysis in which the parameters were assumed to be normally distributed around their mean values. Equations (12) and (13) were only used for evaluation of the uncertainty of flow in the x direction based on Eq. (6). The

procedure for the propagation of the measurement errors of z , h and ρ_a in the calculation of h_f is included in the [Appendix](#).

Results

The deviation between the pressures measured by the barometric pressure logger and water level loggers during the times when they were not submerged (P_{offset}) were near or below the manufacturer-specified accuracy, and no noticeable drift was recorded (Table 1). The loggers in wells 1–1 and 2–8 were notable exceptions though, and had offsets of –3.6 and 1.9 kPa, respectively. The logger in well 3–6 failed in the second half of May 2015 for unknown reasons and no useable results were therefore available for this piezometer. The time lag between the loggers and the computer clock at the time of download in the first week of July (just under 2 months after they were started on 12 May) reached up to 144 s, and all loggers except three lagged behind the computer time (Table 1).

The importance of the effect of the logger time offset on the head difference is illustrated for a single tidal cycle on 7 July 2015 in Fig. 4. Figure 4a shows the freshwater-head-data points for observation wells 3–2 and 3–3, of which the screens are separated vertically by 16.8 m. Two simple harmonic functions (one for each well) fitted through the data points to smooth the data are shown as well. A third curve, the almost imperceptible blue line, represents the smoothed data of well 3–3 but it is shifted in time by 120 s. Figure 4b shows the head difference between the screens of 3–2 and 3–3 based on the original and the time-shifted smoothed curves. This example clearly reveals that the inaccuracies of the datalogger clocks have a large effect on the inferred head difference in terms of the timing of the peaks and troughs as well as on the amplitude.

The density of the water samples obtained by pumping in May 2015 ranged between 999.7 and 1,046.3 kg/m³ (Table 1). The seawater had a density of 1,026.6 kg/m³. A comparison of these laboratory-determined values to those at the depth of the well screen calculated from the downhole conductivity and temperature profiles, showed a linear correlation with a $R^2 = 0.991$ when one outlier was removed. The outlier was the sample from well 2–4, which had a much lower conductivity and density than the maximum values recorded using the downhole measurements. This is attributed to the stratification of the water column along the 6 m well screen (Fig. 5). The specific conductance of the water sample was less than then mean specific conductance of the water column averaged over the length over the well screen. Such sample bias towards the fresher groundwater along the screen has been described previously by Kohout and Hoy (1963).

A pronounced salinity stratification was apparent in the water columns inside essentially all wells, except the shallow ones with the freshest water. The electrical conductivity values were lowest in the upper part of the water column, and

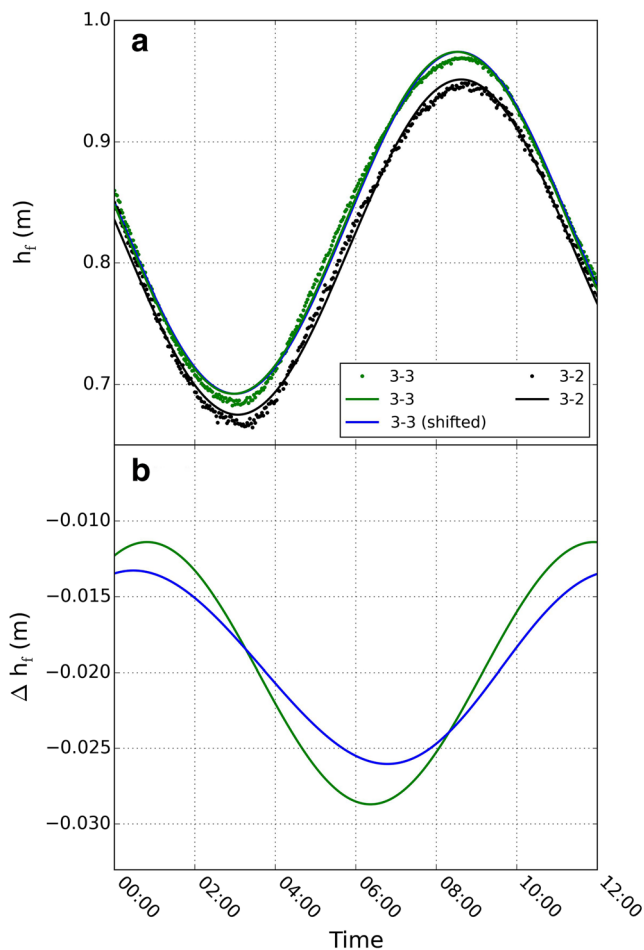


Fig. 4 Graphs showing **a** freshwater head versus time and **b** the freshwater head difference versus time, for piezometers 3–2 and 3–3 on 7 July 2015. The measurements are shown as data points the upper graph and corresponding smoothed curves fitted to the data are shown as green and black lines. The blue line in the upper graph represents the smoothed data of 3–3 shifted in time by 2 min, but it is barely visible at this scale

increased in a step-wise fashion with depth. An extreme example was well 1–4 at site 1, which when sampled had a salinity almost equal to that of the seawater, but became filled entirely with freshwater during the weeks following sampling (Fig. 6a). Well 2–8 is an example of a well that was saline but only showed a moderate degree of stratification (Fig. 6b), while 2–7 showed significant freshening in the top 20 m of the water column (Fig. 6c). A comparison between the data collected on 3 July and 5 August shows that the stratification remained relatively stable with time for these monitoring wells.

The observed stratification is in no way representative for the salinity distribution in the aquifer. It is a consequence of the improper sealing of the threaded PVC joints of the piezometer casing, despite the use of O-ring seals. Inspection with a downhole camera demonstrated the presence of leaks, which are made visible by precipitates, presumably of carbonate minerals, along the inner wall of the piezometers (Fig. 7). In some cases, the precipitates appear to have grown vertically

upward from the openings at the joints (Fig. 7), suggesting that there may be a net upward component of the flow inside the piezometer. A more detailed characterisation of these features remains required however to establish this with certainty.

All observation wells showed a pronounced response to the semi-diurnal tidal fluctuations in the open sea, except for observation well 3–1, which only responded to the monthly spring-neap cycle. The maximum difference between low and high tide could be as high as 1 m for the observation wells at site 1 (Fig. 8), but due to damping effects, the amplitudes were lower at sites 2 and 3. The general increase of the groundwater density with depth, makes that the values of *h* decreased with increasing screen depth (compare 1–3 and 1–5 in Fig. 8, with screen bottom depths of –24.6 and –50.1 m AHD, respectively), as expected.

Fitting the time series measured by the loggers through the data points of the manual water-level measurements (step 7 in section ‘Conversion to freshwater head’) yielded a residual for

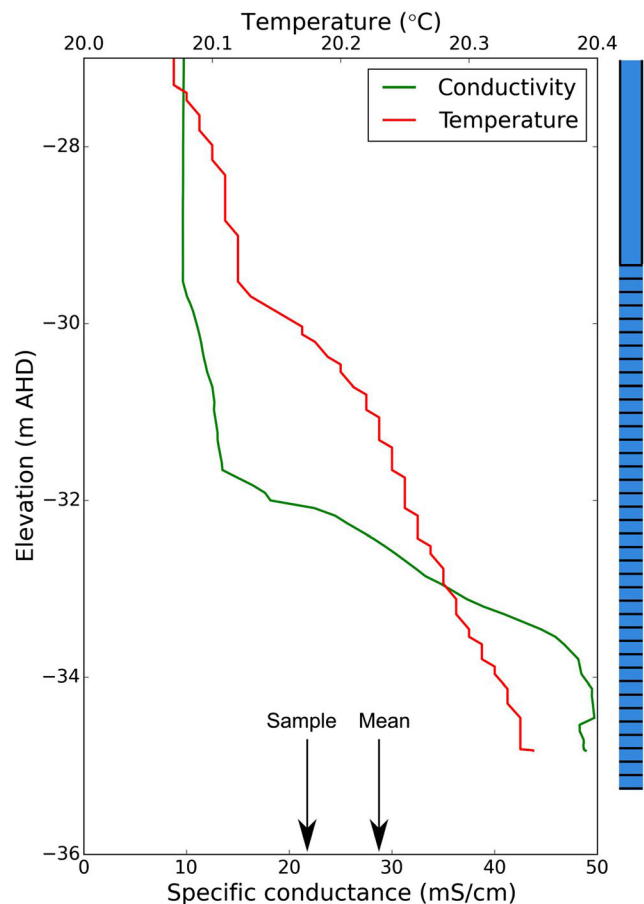


Fig. 5 Graph showing the variation of specific conductance and temperature along the deepest part of observation well 2–4. The mean specific conductance of the water column as well as that of the sample taken by pumping in May 2015 are indicated on the lower horizontal axis. The position of the well screen is indicated on the right-hand side of the graph, which was 6 m in length and straddled the fresh groundwater/saline-water interface

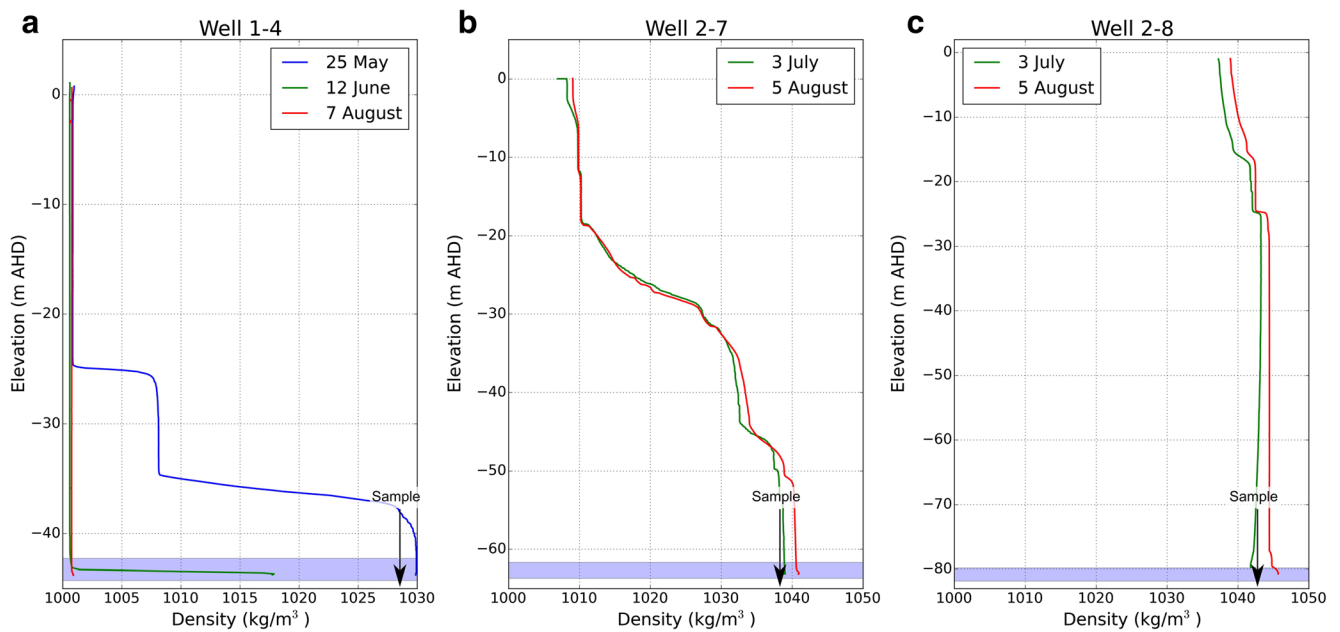


Fig. 6 Graphs showing the change of the density of the water column inside the piezometer with elevation for different days during the measurement period for observation wells **a** 1–4, **b** 2–7 and **c** 2–8. The

arrows on the horizontal axis point to the density that was measured on the water sample taken in May 2015. The light-blue-shaded areas indicate the screen interval

each of the manual water-level measurements. The mean of the absolute value of the residuals was 0.016 m, with a maximum of 0.06 m. Unexpected higher (> 0.1 m) deviations were observed for the wells at site 2 for the readings taken on 3 July 2015. It is suspected that these are due to operator error and may have been caused by incorrect reporting of the time (not taking into account the correct daylight savings setting) or by reading the measurement tape at the wrong decimal mark. Since this could not be established with certainty, these measurements were therefore excluded from the analysis. The standard deviation of the residuals is reported in Table 1 and

is considered to be a measure for the composite measurement accuracy of the water levels. The standard deviations ranged between 0.0018 and 0.05 m, with an average of $\sigma_h = 0.02$ m ($n = 105$).

The change of the salinity of the water column inside the well with time severely complicated the conversion of the measured heads to equivalent freshwater heads because it made ρ_a (Eq. 2) become a function of time. This was clearly observed by a linear trend in the measured water level of well 1–4 during the first 3 weeks of the measurement period, where there was a much higher water level in this well than in the

Fig. 7 Photographs made using a downhole camera in piezometers 1–6 (**a–b**) and 1–7 (**c–d**). The photographs in the upper row are taken vertically down, the two in the lower row are facing sideways via a sideview camera 90° to the main camera. The approximate location of the details (in **b** and **d**) are shown by a black ellipse (in **a** and **c**)

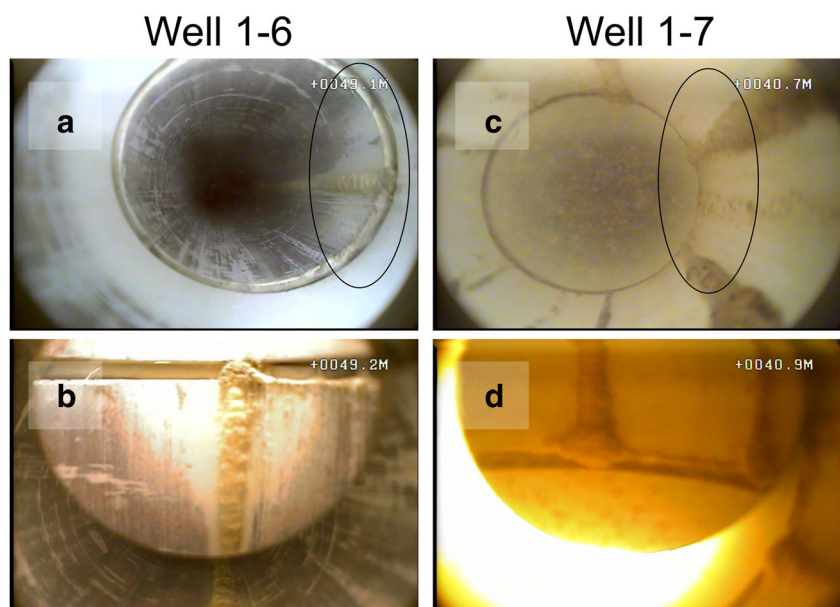


Fig. 8 Graph showing the measured hydraulic heads (m AHD) for three piezometers at site 1 between 12 May and 13 June 2015. The density of the water column inside piezometers 1–5 and 1–3 remained almost constant during this period, whereas that of piezometer 1–4 decreased due to the inflow of fresher water. As a consequence, the head measured in the latter increased during a 2–3-week period, and remained relatively high

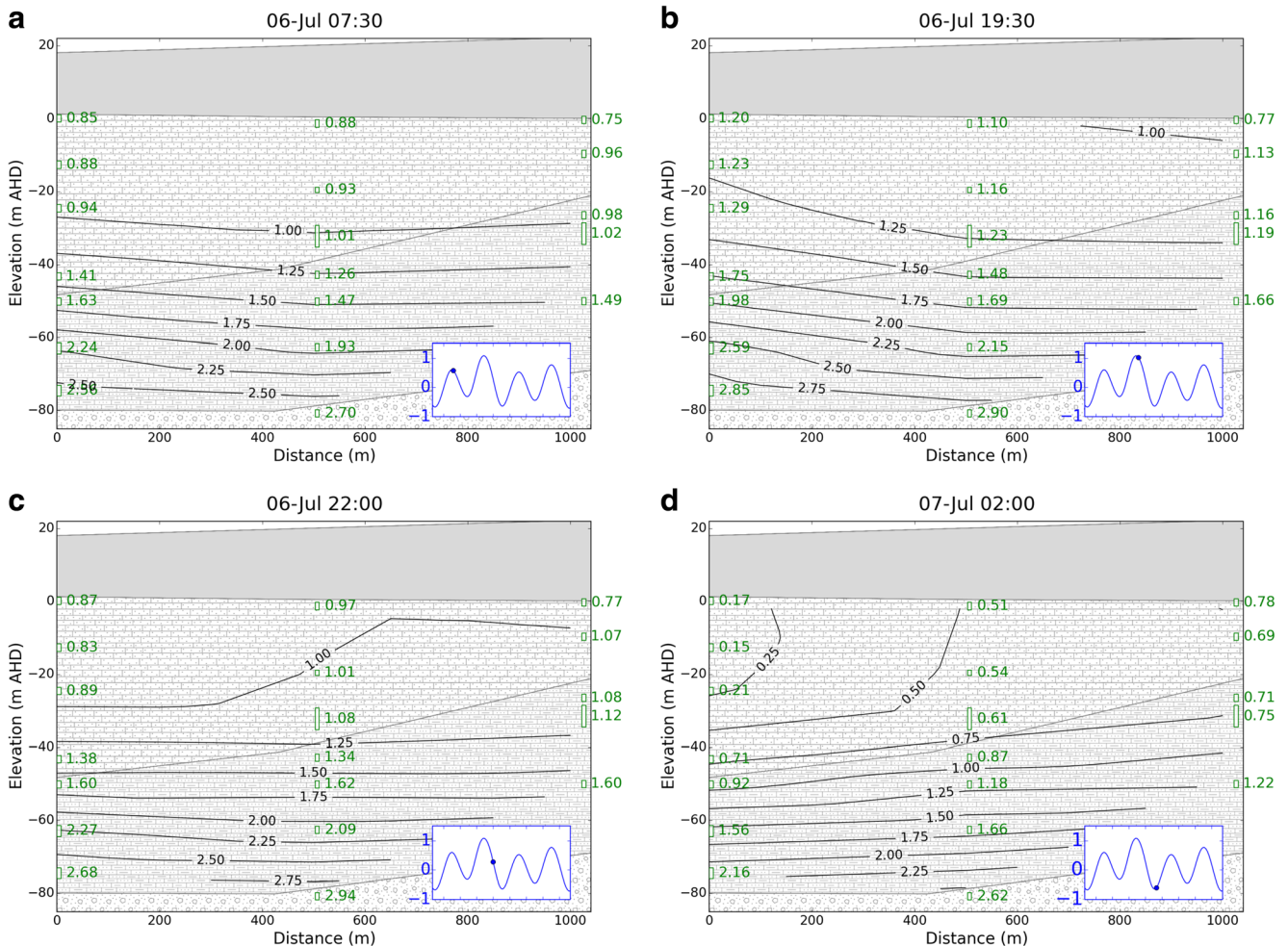
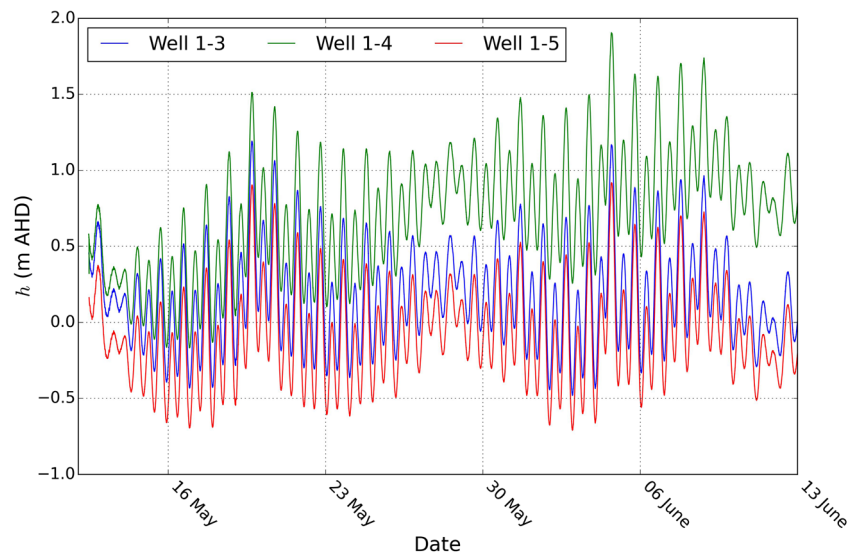


Fig. 9 Cross-sectional plots showing the contour lines of equal freshwater head at **a** 07:30 6 July, **b** 19:30 6 July, **c** 22:00 6 July and **d** 02:00 7 July. Freshwater head values based on the measurements are indicated in green font next to the well screen. The labels of the

contours lines are in black. The inset graphs show the variation of the sea level around the mean for the period 00:00 6 July to 02:00 8 July in units of meters

other wells at site 1 (Fig. 8). Because of the aforementioned technical difficulties with the downhole instrument, the variation of ρ_a was not known with sufficient accuracy at all times during the measurement period. Therefore, a detailed analysis of the horizontal and vertical flow components was only attempted for the days 6 and 7 July 2015. These days were chosen because they followed shortly after reliable downhole measurements were completed.

The resulting values of the freshwater heads are shown as contour plots in Fig. 9 at various points in time. An animation showing the changes of the heads with time at 30 min intervals has been provided as electronic supplementary material (ESM) to this article. It should be emphasised that no inferences about vertical flow can be made from the contour lines of equal freshwater head, but changes of the freshwater head along a horizontal line of the same elevation are indicative of horizontal flow, with the flow being directed from high to low freshwater head values. It can be inferred that the horizontal flow component between sites 1 and 2 is seaward in the upper part of the aquifer ($z > -30$ m AHD) for most of the time except during the highest tidal levels on 6 July (Fig. 9b). In the deeper parts of the aquifer, the horizontal flow alternates between landward during high tide and seaward during low tide. Between sites 2 and 3 the flow is seaward more frequently and across a greater depth interval of the aquifer, although the flow direction reverses from seaward to landward shortly before the tide reaches its highest level on July 6 (Fig. 9b). Seaward flow is resumed just before the lowest level is reached during the subsequent falling tide. The figure also highlights that the horizontal freshwater head gradients are much higher in the upper than in the lower part of the aquifer, which points at lower flow rates in the saltwater body than in the freshwater above it. This has been noted in other studies as well and is related to the fact that the flow of saltwater is driven primarily by the dispersive losses along the freshwater–saltwater transition zone (Cooper 1959).

The net horizontal flow at a particular elevation over a tidal cycle (defined as the period between subsequent low tides) can be determined by integrating the value of the horizontal component of the specific discharge with respect to time t :

$$V_w = \int q_x dt = \int -K_x \frac{dh_f}{dx} dt \tag{14}$$

where V_w is the volume of water displaced during a tidal cycle per unit of cross-sectional area (m). Because dh_f/dx is a function of elevation z , so is V_w and because the variation of K_x with depth is unknown, the parameter that was evaluated instead was

$$\beta = -\frac{V_w}{K_x} = \int \frac{dh_f}{dx} dt \tag{15}$$

which has the units of days. A negative value of β indicates seaward flow, whereas a positive value indicates landward flow. The variation of β as a function of elevation z is shown in Fig. 10

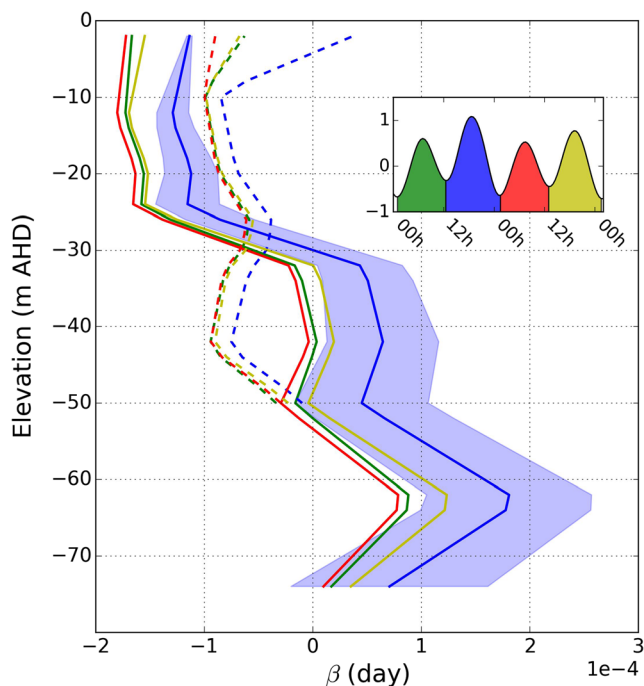
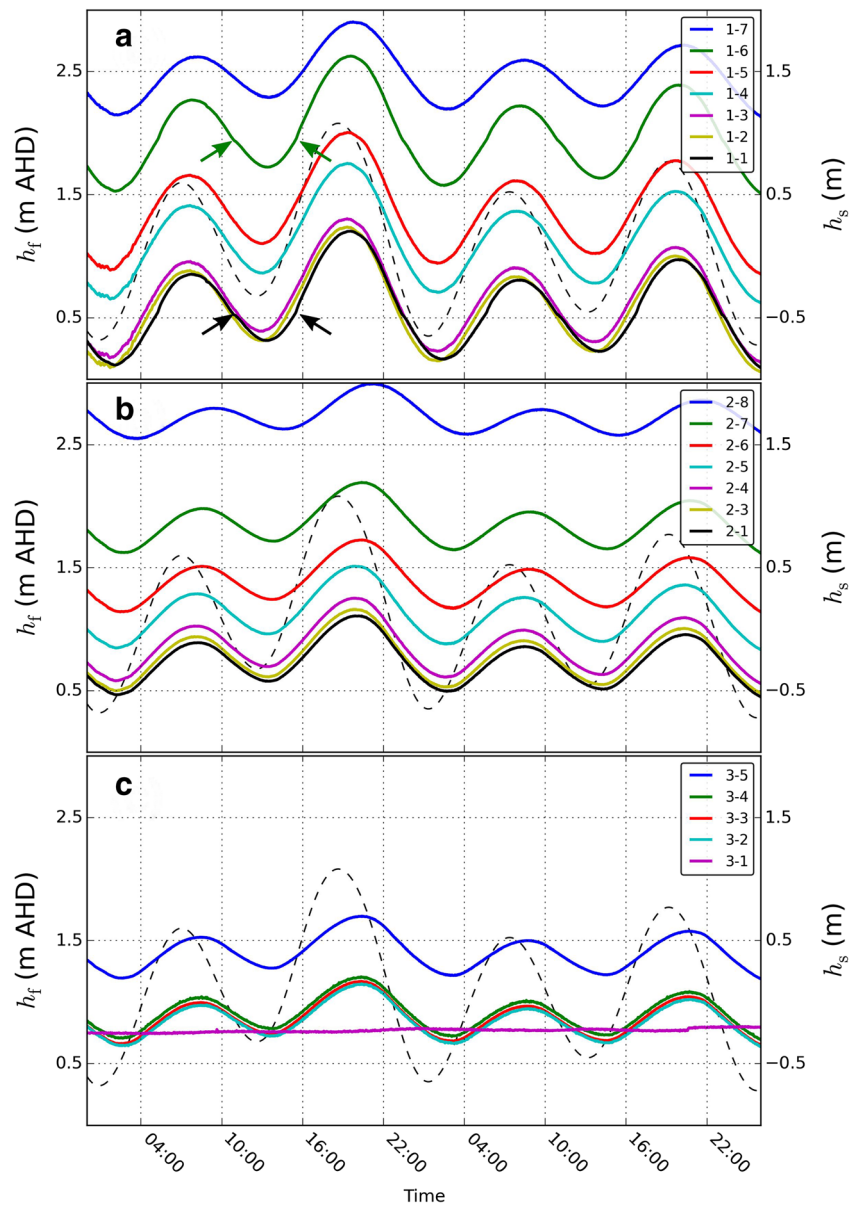


Fig. 10 Graph showing the value of β as a function of elevation for four subsequent tidal cycles on 6 and 7 July 2015. Solid and dashed lines are for the freshwater head difference between sites 1 and 2, and sites 2 and 3, respectively. Negative values of β indicate net flow towards the sea, positive values indicate net landward flow. The inset graph shows the variation of the sea level around the mean for the period 00:00 6 July to 02:00 8 July in units of metres. The colours below the curve indicate the ~12-h period between low tides and correspond to the colours of the lines in the main graph. The wide light-bluish band in the main graph represents the uncertainty of β between sites 1 and 2 for tidal cycle 2

for the four tidal cycles that occurred on 6 and 7 July. The results corroborate the trends visible in Fig. 9, and show that between sites 1 and 2, there is a net component of seaward flow of groundwater above an elevation of approximately $z > -30$ m AHD. The net flow appears to be almost zero between $-50 < z < -30$ m AHD, except during the second tidal cycle. Landward flow dominates where $z < -50$ m. Between sites 2 and 3, net seaward flow occurs across the entire depth interval along which dh_f/dx could be evaluated during all four tidal cycles. The only exception is the second tidal cycle, when landward flow appears to be occurring where $z > -5$ m AHD. It should be recalled that the value of β is only indicative of the direction of the flow, not the magnitude.

The freshwater heads as a function of time are shown in the graphs of Fig. 11. The high groundwater salinity in the deeper part of the aquifer resulted in a distinct increase of the freshwater heads with depth. For the shallower screens, the correction terms due to density effects were smaller, and the difference of the freshwater head values between the screen locations was smaller. Unlike the other wells, the water levels in well 3–1 did not show a response to the semi-diurnal tide. For wells 1–6 and 1–1, a distinct change in the slope of the curves

Fig. 11 Graphs showing the variation of the freshwater heads for the period 00:00 6 July to 02:00 8 July for **a** site 1, **b** site 2, and **c** site 3. Black and green arrows (**a**) indicate examples of where breaks in slope occur for observation wells 1–1 and 1–6, respectively. The dashed line is the measured tide level over the observation period



is noticeable, which occurred during the rising and falling tide, and always at the same freshwater head value.

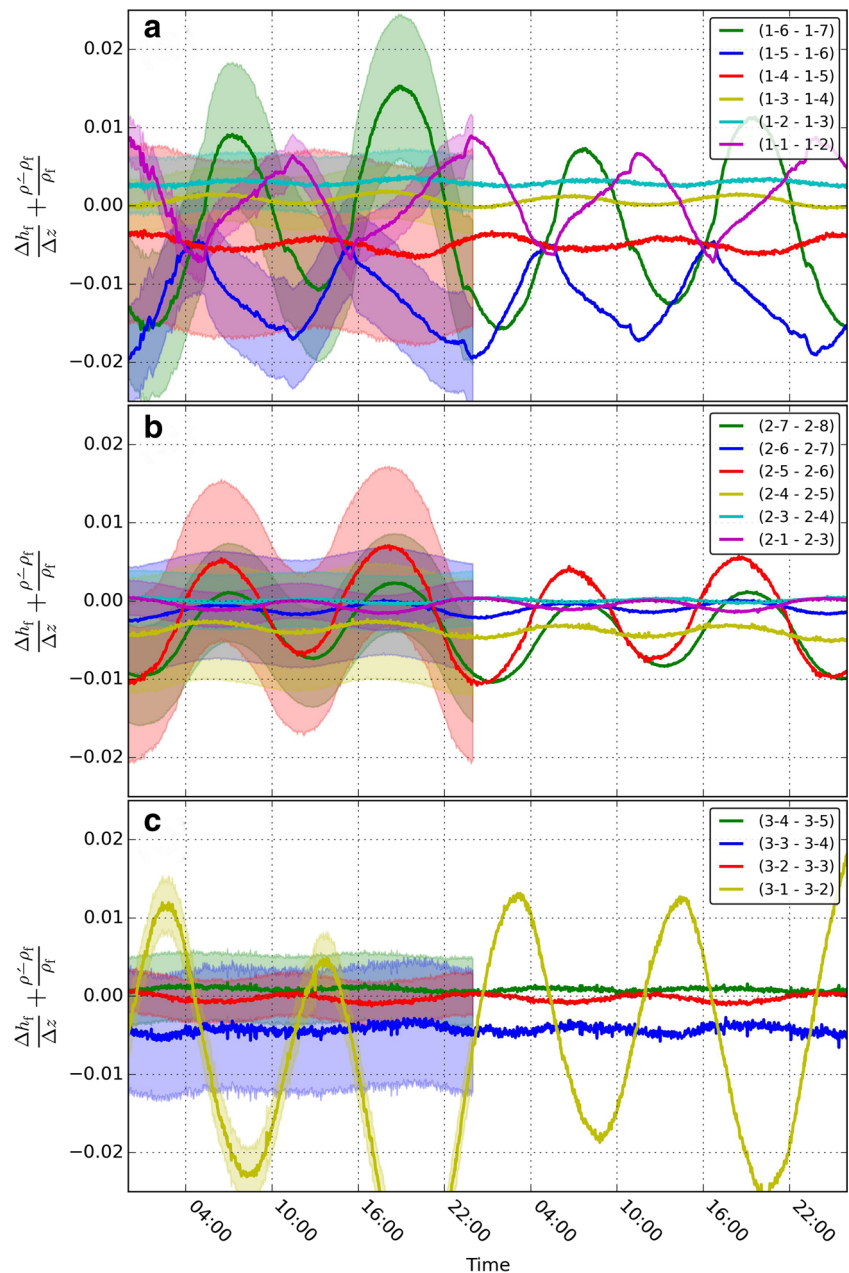
This change in slope has a strong effect on the curves that show the driving force term for vertical flow, the term in square brackets in Eq. (7), in Fig. 12, in particular the curves that show the gradient between wells 1–5 and 1–6, and 1–1 and 1–2. Most curves fluctuate sinusoidally around a mean of 0, albeit that some are offset from this value. The uncertainty bands, representing 1SD (standard deviation) above and below the curve, are plotted as translucent bands with the same colour as the curve for the data on 6 July only. The bands are not shown for the data on 7 July to avoid making the graph too crowded. The time-averaged values of $-\Delta h_f / \Delta z$ are plotted versus $(\rho' - \rho_f) / \rho_f$ in the scatter diagram of Fig. 13. The white line indicates where the points would lie if the net vertical flow component would be 0 (which would be equivalent to

hydrostatic conditions in a non-tidal system, cf. Eq. 10). All data points lie within close proximity of this line, although there is a tendency for them to plot within the region of upward flow. The error bars, representing the standard deviations of the $-\Delta h_f / \Delta z$ and $(\rho' - \rho_f) / \rho_f$ terms show, however, that most of the deviations are not significant, which will be discussed in greater detail in the following section.

Discussion

The difficulties associated with the collection of the data in the field made inferring the vertical and horizontal flow patterns based on the measured heads a tedious and onerous procedure. The pressure loggers were also found to have a significant time offset, reaching up to 3 min after less than 2 months of

Fig. 12 Graphs showing the variation of the driving force for vertical flow for the period 00:00 6 July to 02:00 8th July for **a** site 1, **b** site 2, and **c** site 3. The error bands on 6 July indicate the uncertainty expressed by 1SD above and below the curve



operation. This necessitated an extra post-processing step of the data to shift the time series, as such time shifts can propagate as significant errors on the calculated gradients in this system where heads fluctuate at the timescale of the semi-diurnal tidal cycle (Fig. 4). Some loggers deployed (but not used in this article) had clocks that failed at random times, causing erroneous timestamps to be recorded from which moment onward the data series became unusable. Finally, one logger showed anomalous drift after a few weeks of operation.

A major task was the quantification of the average density of the water column inside the observation wells, which was time-consuming, necessitated the removal of the pressure loggers from the well, and was plagued by technical issues with

the downhole sonde. These were caused by water entering the sonde's interior, which was found to become a serious problem at water depths over ~50 m. On each occasion, this meant that the sonde had to be disassembled, dried completely and recalibrated.

The leaking wells severely limited the usability of the collected pressure data, because it meant that the density inside the well varied with time in an unknown way. The leaks were caused by improper placement of the O-rings insufficient PVC-glue between the threaded PVC casing joints and tightness of the threaded joint by the driller, and could be clearly identified on downhole camera photographs (Fig. 7). It is contended that many boreholes in coastal and inland settings

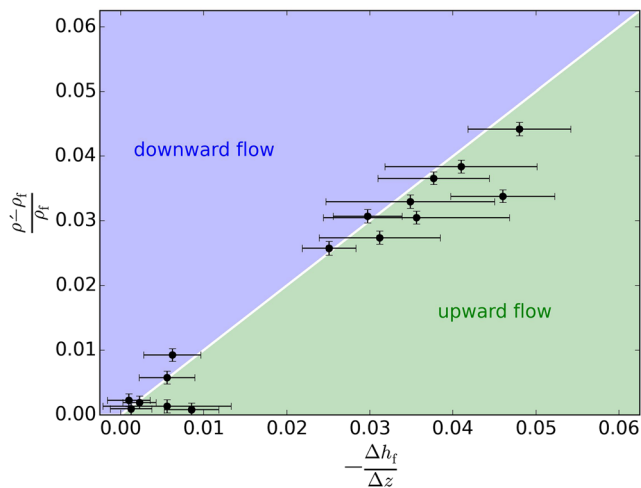


Fig. 13 Scatter plot showing the mean values of $-\Delta h_f/\Delta z$ for the period 00:00 6 July to 02:00 8 July versus $(\rho' - \rho_f)/\rho_f$. The white line separating the blue and green regions indicates where the data points would lie in case there was no net vertical flow. The horizontal and vertical error bars represent the standard deviations of the $-\Delta h_f/\Delta z$ and $(\rho' - \rho_f)/\rho_f$ terms, respectively as determined by Monte Carlo analysis

suffer from salinity stratifications of the water column inside the well due to similar improper installation, or leaks caused by cracking and corrosion of the casing; however, even non-leaking intact wells can have salinity stratifications, as was already noted by Kohout (1961) in the classical early work on the Biscayne aquifer in Florida. These are caused by fluctuations of the salinity of the groundwater at the well screen, which, depending on the aquifer's permeability, can be occurring over the period of days to weeks in response to recharge events. These temporal changes of salinity of the groundwater cause a change of the salinity of the water column inside the well, either due to water flowing across the screen, or by diffusion of dissolved salts.

This means that the salinity inside the observation well must always be verified using a downhole measurement tool, in particular because the average density of the water column, ρ_a , is one of the most sensitive parameters controlling the uncertainty of the freshwater head (h_f). An uncertainty was assigned to ρ_a by comparing differences of the density in the bottom of the wells between July and August (Fig. 6), which were expected to change only minimally by natural causes. It was inferred that a standard deviation of $\sigma_\rho = 1 \text{ kg/m}^3$ would be appropriate. This choice is rather subjective, but since the real value cannot be known, it was deemed the most justified way.

The uncertainty of the freshwater head is further a function of the measurement error of the depth of the bottom of the well screen (z_i) and the hydraulic heads determined using the pressure transducers (h). The measurement of the well depth was deemed to be accurate within 0.01 m, but because the borehole may not be perfectly straight, it was decided to adopt a relatively high standard deviation of $\sigma_z = 0.01 \text{ m}$. The standard

deviations of the residuals between the logger time series and the manual measurements are listed in Table 1. Their average is 0.022 m, and based on this it was decided to adopt $\sigma_h = 0.02 \text{ m}$.

Using the error propagation rules shown in the Appendix, these values of σ_ρ , σ_z and σ_h resulted in a standard deviation for the freshwater head values of $0.021 < \sigma_{h_f} < 0.083 \text{ m}$. The values increase with z_i , which is expected as the second term in Eq. (5) becomes dominant relative to the first term with larger z_i . The uncertainty of h_f was taken into consideration when evaluating the dh_f/dx terms to derive the graph of β versus z (Fig. 10). The uncertainty band is shown only for the flow between sites 1 and 2 for tidal cycle 2 in order to not clutter the graph. It was obtained by applying Eqs. (12) and (13) to the dh_f/dx term, with σ_{h_f} being a simplified function of z according to $\sigma_{h_f} = -z/1,250$. This results in a widening uncertainty band that provides an estimate of the significance of the value of β .

Based on this analysis of the freshwater head gradients in the horizontal direction, it is possible to infer that there was net horizontal flow of freshwater towards the coast in the upper part of the PWF during the four tidal cycles analysed, apparent from a negative value of β in Fig. 10. Figure 9 further illustrates how the magnitude and direction of dh_f/dx varied with the tidal cycle. The flow became almost stagnant during the high tide of the first tidal cycle on 6 July 2015, but reversed to landward flow during the much stronger second high tide on that day. In the saltwater part of the aquifer at greater depth ($-50 > z > -80 \text{ m AHD}$, the horizontal gradient of the freshwater head between sites 1 and 2 shows a regular alternation with the tidal cycle. The values of β show that the net flow was close to zero in the interval $-30 > z > -50 \text{ m AHD}$, but a net landward component was inferred below $z < -50 \text{ m AHD}$ (Fig. 10). More landward, between sites 2 and 3, the flow across the entire monitored depth of the aquifer for which data were available (up until $z = -50 \text{ m AHD}$), the flow was towards the coast.

These observations are consistent with the model of Cooper (1959) and thus confirm the general validity of the conceptual model of circulatory flow within the seawater wedge and freshwater flowing towards the coast above and over it. It is suspected though, that a component of net vertical upward flow exists in the bottom part of the aquifer, because of the presence of the hypersaline groundwater, which is also known to occur in the Maslin Sands aquifer underlying the PWF (Irvine 2016). However, due to the large uncertainty associated with the calculated values of the driving force it was not possible to infer the net vertical flow component over the 4 tidal cycles with any degree of confidence. This is due to the uncertainty involved in the quantification of the various terms in Eq. (7).

However, even under non-tidal, constant-density conditions, resolving vertical fluxes using piezometer head data is

often intractable, which is illustrated by the following simple example. If it is assumed that $\sigma_h = \sigma_z = 0.01$ m, it follows from Eq. (12) that the uncertainties of the Δ terms in Eq. (11) become $\sigma_{\Delta h} = \sigma_{\Delta z} = 0.014$ m. For an aquifer that has $q_z = 1$ mm day⁻¹ and $K_z = 1$ m day⁻¹, it follows that $\Delta h/\Delta z = i_z = 0.001$; hence, if $\Delta z = 10$ m, $\Delta h = 0.01$ m and the right-hand side of Eq. (13) becomes 1.4. This means that the relative uncertainty is 140%, and thus the range of probable values of the gradient, i.e. those enclosed by ± 1 SD, can be positive, negative or zero. This outcome leads to a rather startling conclusion that under a wide range of conditions it is not possible to infer vertical flow from head measurements with any degree of confidence. This is confirmed by the findings of Silliman and Mantz (2000) who found that the measurement error was too large to reliably predict the vertical head gradient in the datasets used for their study.

To establish if there is a vertical flow component in a variable-density system, the condition that needs to be tested is if $-\Delta h/\Delta z$ deviates significantly from $(\rho' - \rho_f)/\rho_f$ (cf. Eq. 10). A graphical interpretation is shown in the graph in Fig. 13, which shows the values of $-\Delta h/\Delta z$ versus $(\rho' - \rho_f)/\rho_f$. The solid white line indicates where the data points would plot if there was no net vertical flow (cf. Eq. 10), i.e., the equivalent of a hydrostatic situation for nontidal conditions. Even though the majority of the data points plots in the region of upward flow, the fact that practically all the error bars, which represent 1SD on either side of the data point, intersect with the white line shows that the vertical gradient of the freshwater head could not be determined with sufficient accuracy. So while the results show that there is a periodic reversal of the vertical flow component, no conclusions can be drawn about any net vertical flow.

The inaccuracy of the head-based flow estimates poses a severe limitation to developing more refined conceptual models of groundwater flow within and near the freshwater–saltwater interface. In the case of the present study, it meant that it was impossible to ascertain if the presence of the hypersaline groundwater is due to net upward migration. Moreover, the potential presence of multiple circulation cells in a stratified saltwater wedge, which has been inferred from laboratory and numerical experiments (Oz et al. 2011, 2014), will not be identifiable in the field without more accurate flow measurements.

The study of Acworth (2007) found that conditions were close to hydrostatic near a coastal creek, except for a conspicuous jump in the head profiles at the depth of the freshwater–saltwater interface. A propagated error of the salinity measurement was ruled out as the cause for this jump, but an explanation in terms of a hydraulic process could not be provided. Kim et al. (2006) conducted flowmeter tests in fully screened boreholes on Jeju Island in Korea and found that the direction of the flow reversed over a tidal cycle. Yet, there was no corresponding reversal of the direction of the gradient of the hydraulic

head. This inconsistency is likely explained by the use of long well screens, or a density stratification inside the boreholes. These examples, as well as the present study highlight the need for comprehensive error analysis and uncertainty estimation so that it can be assessed if inferred flow patterns are significant, or within the range of uncertainty of the method used.

Finally, the variable density of the water column inside observation wells, whether caused by leaks or other factors, shows that the height of the water column is an inaccurate indicator of the groundwater pressure at the elevation of the well screen. This problem can be circumvented by deploying the pressure transducers at the screen (Gibbes et al. 2007), but the loggers must then have a greater measurement range and this makes them less accurate. The problems encountered can therefore only be solved by better instruments and more sophisticated experimental designs.

Conclusions

This study aimed to determine the groundwater flow pattern in a semi-confined coastal aquifer using a dense grid of hydraulic head measurements along a shore-perpendicular transect in the town of Aldinga Beach in Australia. The analysis was severely complicated by the tidal dynamics, variable-density effects and measurement difficulties. The greatest difficulty encountered in this study was determining the density of the water column inside the observation well, which was both due to instrumental problems and leaking well casings. It is believed that salinity variations with observation wells are common in all coastal areas, and its effect must be quantified for all head-based analyses of groundwater flow, including numerical studies in which head data are used for calibration.

The horizontal and vertical components of the flow were analysed separately. By estimating the accuracy of the measurements and applying error propagation, the uncertainty of the flow components was quantified. It was found that there was net seaward horizontal flow in the upper part of the aquifer during the period analysed. The vertical flow direction was found to alternate with the tide, but a net vertical flow direction could not be established due to the large uncertainty, in particular of the vertical gradient of the freshwater head.

The comprehensive analysis highlights that head-based quantification of groundwater flow is inaccurate to the degree that the flow components within aquifers, especially in the vertical direction, are essentially impossible to measure with common measurement procedures. This problem is especially severe under variable-density conditions, but has also been recognised for constant-density systems (Silliman and Mantz 2000; Devlin and McElwee 2007). The profound implication that there is a blunt tool in the hydrogeologist's toolbox is not often acknowledged though, yet it means that we lack a reliable method to address the fundamental problem of measuring

groundwater flow. While some improvements to the experimental setup such as deployment of pressure transducers in the well screens, could have been made in the present study, the accuracy improvement would still not have sufficed to determine the vertical flow component. This problem can only be solved by better measurement technologies and dedicated instrumental design.

Acknowledgements Michael Teubner is thanked for his advice on the uncertainty analysis. Scott Prinos and an anonymous reviewer are thanked for their comments, which helped to improve the manuscript.

Funding Information This study was supported by funding from the Australian National Collaborative Research Infrastructure Scheme.

Appendix: Error propagation in the calculation of freshwater head

The freshwater head is calculated as

$$h_f = \frac{\rho_a h - \rho_a - \rho_f}{\rho_f} z \quad (16)$$

where ρ_a is the average density of the water column (kg/m^3), h (m) is the hydraulic head, ρ_f is the freshwater density (kg/m^3), and z is the elevation of the bottom of the observation well (m, expressed relative to AHD). Equation (16) can be written as

$$h_f = a - c \quad (17)$$

where

$$a = \frac{\rho_a h}{\rho_f} \quad (18)$$

$$b = \frac{\rho_a - \rho_f}{\rho_f} \quad (19)$$

$$c = bz \quad (20)$$

Denoting the standard deviations of ρ , h and z as σ_ρ , σ_h , σ_z , respectively, and with ρ_f a constant, the standard deviations of the a , b and c terms become

$$\sigma_a = |a| \sqrt{\left(\frac{\sigma_\rho}{\rho_a}\right)^2 + \left(\frac{\sigma_h}{h}\right)^2} \quad (21)$$

$$\sigma_b = |b| \sqrt{\left(\frac{\sigma_\rho}{\rho_a - \rho_f}\right)^2} \quad (22)$$

$$\sigma_c = |c| \sqrt{\left(\frac{\sigma_b}{b}\right)^2 + \left(\frac{\sigma_z}{z}\right)^2} \quad (23)$$

and finally

$$\sigma_{h_f} = \sqrt{\sigma_a^2 + \sigma_c^2} \quad (24)$$

References

- Abarca E, Carrera J, Sánchez-Vila X, Dentz M (2007) Anisotropic dispersive Henry problem. *Adv Water Resour* 30:913–926
- Acworth RI (2007) Measurement of vertical environmental-head profiles in unconfined sand aquifers using a multi-channel manometer board. *Hydrogeol J* 15:1279–1289
- Adelaide and Mount Lofty Ranges NRM Board (2007) Water allocation plan for the McLaren Vale Prescribed Wells Area. Adelaide and Mount Lofty Ranges NRM Board, Adelaide, Australia, 46 pp
- Australian Bureau of Meteorology (2015) Climate data online. <http://www.bom.gov.au/climate/data/>. Accessed 1 Dec 2015
- Baldock TE, Baird AJ, Horn DP, Mason T (2001) Measurements and modeling of swash-induced pressure gradients in the surface layers of a sand beach. *J Geophys Res Oceans* 106:2653–2666
- Bowers DG, Lennon GW (1990) Tidal progression in a near-resonant system: a case study from South Australia. *Estuar Coast Shelf Sci* 30:17–34
- Bye JAT, Narayan KA (2009) Groundwater response to the tide in wetlands: observations from the Gillman Marshes, South Australia. *Estuar Coast Shelf Sci* 84:219–226
- Chang SW, Clement TP (2013) Laboratory and numerical investigation of transport processes occurring above and within a saltwater wedge. *J Contam Hydrol* 147:14–24
- Cooper HH (1959) A hypothesis concerning the dynamic balance of fresh water and salt water in a coastal aquifer. *J Geophys Res* 64:461–467
- Cooper HH (1964) Preface. In: *Sea water in coastal aquifers*. US Geol Surv Water Suppl Pap 1613-C, C71–C84
- Cooper BJ (1979) Eocene to Miocene stratigraphy of the Willunga embayment / by B.J. Cooper; with an appendix. Notes on Ostracoda from Willunga embayment boreholes WLG38, WLG40 and WLG42 by K.G. McKenzie. Govt. Pr, Adelaide, Australia
- Davies PB (1987) Modeling areal, variable-density, ground-water flow using equivalent freshwater head: analysis of potentially significant errors. In: *Proceedings of NWWA conference on solving groundwater problems with models*, Denver, CO, February 1987, pp 888–903
- Devlin JF, McElwee CD (2007) Effects of measurement error on horizontal hydraulic gradient estimates. *Ground Water* 45:62–73
- Gibbes B, Robinson C, Li L, Lockington D (2007) Measurement of hydrodynamics and pore water chemistry in intertidal groundwater systems. *J Coast Res* 50:884–894
- Henry HR (1964) Effects of dispersion on salt encroachment in coastal aquifers. In: Cooper HH (ed) *Sea water in coastal aquifers*. US Geol Surv Water Suppl Pap 1613-C, pp 70–81
- Hodgkinson J, Cox ME, McLoughlin S (2007) Groundwater mixing in a sand-island freshwater lens: density-dependent flow and stratigraphic controls. *Aust J Earth Sci* 54:927–946
- In-Situ Inc. (2013) Operator's manual Level TROLL® 300, 500, 700, 700H instruments. In-Situ, Fort Collins, CO, 84 pp
- Irvine ML (2016) Using tracers to determine groundwater fluxes in a coastal aquitard-aquifer system. MSc Thesis, Flinders University, Adelaide, Australia
- Kim, K.-Y., Seong, H., Kim, T., Park, K.-H., Woo, N.-C., Park, Y.-S., Koh, G.-W., Park, W.-B., 2006. Tidal effects on variations of fresh-saltwater interface and groundwater flow in a multilayered coastal aquifer on a volcanic island (Jeju Island, Korea). *Journal of Hydrology*, 330(3): 525-542. <https://doi.org/10.1016/j.jhydrol.2006.04.02>
- Kohout FA (1960) Cyclic flow of salt water in the Biscayne aquifer of southeastern Florida. *J Geophys Res* 65:2133–2141
- Kohout FA (1961) Fluctuations of ground-water levels caused by dispersion of salts. *J Geophys Res* 66:2429–2434
- Kohout FA, Hoy ND (1963) Some aspects of sampling salty ground water in coastal aquifers. *Ground Water* 1:28–43

- Lee C-H, Cheng RT-S (1974) On seawater encroachment in coastal aquifers. *Water Resour Res* 10:1039–1043
- Luszczynski NJ (1961) Head and flow of ground water of variable density. *J Geophys Res* 66:4247–4256
- Luszczynski NJ, Swarzenski WV (1966) Salt-water encroachment in southern Nassau and southeastern Queens counties, Long Island, New York. *US Geol Surv Water Suppl Pap* 1613-F
- McKinney W (2010) Data structures for statistical computing in Python. In: *Proceedings of the 9th Python in Science Conference*. Austin, TX, July 2010, pp 51–56
- Michael HA, Mulligan AE, Harvey CF (2005) Seasonal oscillations in water exchange between aquifers and the coastal ocean. *Nature* 436:1145–1148
- Oliphant TE (2007) Python for scientific computing. *Comput Sci Eng* 9:10–20
- Oz I, Shalev E, Gvirtzman H, Yechieli Y, Gavrieli I (2011) Groundwater flow patterns adjacent to a long-term stratified (meromictic) lake. *Water Resour Res* 47:W08528
- Oz I, Shalev E, Yechieli Y, Gavrieli I, Gvirtzman H (2014) Flow dynamics and salt transport in a coastal aquifer driven by a stratified salt-water body: lab experiment and numerical modeling. *J Hydrol* 511:665–674
- Post V, Kooi H, Simmons C (2007) Using hydraulic head measurements in variable-density ground water flow analyses. *Ground Water* 45:664–671
- Reynolds JM (2005) *An introduction to applied and environmental geophysics*. Wiley, Chichester, UK
- Segol G (1994) *Classic groundwater simulations proving and improving numerical models*. Prentice-Hall, Old Tappan, NJ
- Silliman SE, Mantz G (2000) The effect of measurement error on estimating the hydraulic gradient in three dimensions. *Ground Water* 38:114–120
- Simpson MJ, Clement TP (2004) Improving the worthiness of the Henry problem as a benchmark for density-dependent groundwater flow models. *Water Resour Res* 40:W01504
- Smith AJ (2004) Mixed convection and density-dependent seawater circulation in coastal aquifers. *Water Resour Res* 40:W08309
- Urish DW, McKenna TE (2004) Tidal effects on ground water discharge through a sandy marine beach. *Ground Water* 42:971–982
- Van Essen Instruments (2004) *TD Diver product manual*. Van Essen, Delft, The Netherlands, 31 pp
- Walt S, Colbert SC, Varoquaux G (2011) The NumPy Array: a structure for efficient numerical computation. *Comput Sci Eng* 13:22–30
- Werner AD, Bakker M, Post VEA, Vandenbohede A, Lu C, Ataie-Ashtiani B, Simmons CT, Barry DA (2013) Seawater intrusion processes, investigation and management: recent advances and future challenges. *Adv Water Resour* 51:3–26
- YSI Inc. (2009) *6-series multiparameter water quality sondes user manual*. YSI, Yellow Springs, OH